Estimation of Power System Inertia: A Comparative Assessment of Measurement-Based Techniques

Eleftherios O. Kontis, Ioanna D. Pasiopoulou, Dimosthenis A. Kirykos,
Theofilos A. Papadopoulos, Grigorios K. Papagiannis

***Abstract*—The increasing penetration of converter-interfaced renewable energy sources (RESs) is expected to reduce the overall system inertia. Additionally, due to the intermittent nature of RESs, the overall inertia of modern power systems will vary significantly during the day, resulting in frequency stability issues. In this uncertain environment, it is important for power system operators to monitor in real-time the overall system inertia. Scope of this paper is to systematically evaluate the performance of the most known measurement-based inertia estimation techniques. These include ARMAX-based methods and methods based on the sliding window concept. Algorithmic details and distinct characteristics of each method are presented and discussed. The effect of several parameters on the accuracy of the examined methods is investigated by means of Monte Carlo simulations. For the analysis both ringdown and ambient data are considered. The performance of the examined methods is evaluated under different network conditions and configurations, using simulation results obtained from a system frequency response model and the IEEE 9-Bus system. The applicability of both approaches is also assessed using laboratory measurements.**

***Keywords*—ARMAX modeling, frequency stability, inertia response, power system dynamics, swing equation.**

I. Introduction

NOWADAYS, due to environmental concerns, synchronous generators (SGs) are replaced by renewable energy sources (RESs), connected to the utility grid via power converters [1]. Consequently, they are mechanically decoupled from the power system frequency and cannot automatically contribute to power system inertia [2].

This research is co-financed by Greece and the European Union (European Social Fund - ESF) through the Operational Programme «Human Resources Development, Education and Lifelong Learning» in the context of the project "Reinforcement of Postdoctoral Researchers – 2nd Cycle" (MIS-5033021), implemented by the State Scholarships Foundation (IKY).

E. O. Kontis, I. D. Pasiopoulou, D. A. Kirykos, and G. K. Papagiannis are with the School of Electrical and Computer Engineering, Aristotle University of Thessaloniki, Thessaloniki 54124, Greece (e-mail: ekontis@ece.auth.gr, ipasiopo@gmail.com, dimkirik@gmail.com, grigoris@eng.auth.gr)

T. A. Papadopoulos is with the Power Systems Laboratory, Department of Electrical and Computer Engineering, Democritus University of Thrace, Xanthi 67100, Greece (e-mail: thpapad@ee.duth.gr)

E. O. Kontis is also with the Department of Electrical and Computer Engineering, University of Western Macedonia, Kozani, 50100, Greece.

Paper submitted to the International Conference on Power Systems Transients (IPST2021) in Belo Horizonte, Brazil June 6-10, 2021.

The increased penetration of converter-interfaced RESs both decreases the overall power system inertia [3] and changes the inertia distribution, leading to the formation of low inertia areas [4]. Additionally, due to the intermittent nature of RESs, the overall system inertia varies significantly during the day, resulting in frequency stability issues [5], [6]. Hence, power system operators shall estimate close to real-time, using wide area monitoring systems (WAMS), the overall inertia of their grids [2], [5], [7]. For this purpose, several inertia estimation techniques have been proposed in the literature.

A statistical approach based on switching Markov Gaussian models is developed in [8], allowing inertia estimation using field measurements and historical data. Linear regression methods are proposed in [9], [10], [11]. To provide accurate results, these methods require real-time information concerning load level and generation mix. An online approach is developed in [12]. Nevertheless, this method requires the injection of probing signals, complicating its implementation.

In [13] a method, based on dynamic regressor extension and mixing, is proposed. However, this approach requires full knowledge of the turbine-governor systems of all SGs. A method to derive system inertia using synchrophasor measurements is proposed in [14]. To provide accurate results, the method requires precise data concerning the magnitude of the disturbance, i.e., active power imbalance. In [15] and [16] system inertia is estimated by utilizing frequency and voltage responses after a disturbance. However, these approaches require the existence of aggregated load models that simulate efficiently the behavior of the total system load during disturbances [16].

To perform satisfactorily, all the above-mentioned methods require, apart from system measurements some additional information concerning power system properties. In the next paragraphs, techniques that provide system inertia using only system measurements are reviewed.

In [17] a procedure to derive system inertia during ringdown, i.e., transient, events is proposed. The method uses active power variation and rate of change of frequency (*RoCoF*) at the onset of the event to compute via the swing equation the system inertia. Considering only data recorded at the onset of the event renders inertia estimation extremely sensitive to noise [18]. To overcome this issue, [6] proposes a more robust approach, that estimates active power and *RoCoF* variations using four sliding windows (SWs). The SWs are used as filters to eliminate measurement error. However, validation results reveal that the method accuracy is affected by the length of the adopted SWs and the noise level [19].

In [2] the use of autoregressive moving average exogenous input (ARMAX) models is proposed to estimate the system inertia using ringdown data, while the application of ARMAX modeling to ambient data, i.e., normal operation data, is discussed in [7]. In both cases, active power and frequency responses are used to develop transfer functions, describing the active power - frequency relationship. Inertia estimates are then determined by processing the parameters of the derived transfer functions. Validation results indicate that the performance of ARMAX models is affected by noise level and mainly by the size of the analysis window. In fact, in many cases, due to inappropriate window size, unstable transfer functions may result, leading to erroneous estimates [2], [7].

Scope of the paper is to systematically evaluate the performance of inertia estimation techniques that are based only on system measurements. Therefore, methods that rely on the sliding window method (SWM) as well as ARMAX-based approaches are considered and compared. The main contributions of the paper are: a) the performance of the most common measurement-based inertia estimation techniques is assessed under different network configurations, using simulation results and laboratory measurements. b) The impact of several parameters on the accuracy of the examined methods is investigated. In particular, the effect of the length of the analysis window, the noise level, the disturbance magnitude and location as well as the RES penetration level on the performance of the methods is quantified through Monte Carlo (MC) simulations. The conducted analysis provides useful insights concerning the application of measurement-based inertia estimation techniques.

II. Theoretical Background

The frequency response of a power system to a power imbalance can be modeled considering the swing equation of an equivalent SG, described as [12], [19]

$$2H\Delta\frac{df(t)}{dt} = \Delta p_m(t) - \Delta p_e(t) - D\Delta f(t). \tag{1}$$

Here H is the inertia constant in s. f is the frequency in p.u.; p_m and p_e are the p.u. mechanical and electrical powers, respectively. Δ denotes that the changes (variations) of f, df/dt, p_m and p_e should be used and not the absolute values [12]. Finally, D is the damping coefficient. The swing equation can be simplified to contain only variables measured on the electrical side of the system by exploiting the slow-changing nature of mechanical power [20]. Indeed, at the beginning of an event, Δp_m can be considered equal to zero [6], [12]. Thus, (1) can be rewritten as

$$2H\Delta\frac{df(t)}{dt} = -\Delta p_e(t) - D\Delta f(t). \tag{2}$$

By applying the Laplace transform on both sides of (2), the following transfer function is derived [2], [12]

$$G(s) = \frac{\Delta F(s)}{\Delta P(s)} = -\frac{1}{2Hs + D} \tag{3}$$

Here, $\Delta F(s)$ and $\Delta P(s)$ represent frequency and active power deviations in the Laplace domain, respectively.

Methods developed in [2] and [12] use (3) to determine the inertia constant of individual SGs as well as the equivalent inertia constant, i.e., H_{sys}, of multi-machine power systems. The latter is defined as

$$H_{sys} = \frac{\sum_{i=1}^{N} H_i S_i}{\sum_{i=1}^{N} S_i}. \tag{4}$$

Here, N is the total number of SGs connected to the grid, H_i and S_i are the inertia constant and the rated power of the i-th SG, respectively. H_i is directly computed from (3).

In many research papers, the swing equation is further simplified by neglecting the impact of damping [6], [17]. Indeed, at the onset of an event, i.e., at $t_0 = 0^+$, the frequency deviation is practically zero [17], i.e., $\Delta f(0^+) = 0$. In this case, the swing equation takes the following form

$$2H\Delta\frac{df(t)}{dt} = -\Delta p_e(t). \tag{5}$$

In this paper, ARMAX models, that determine inertia via (3), and methods that utilize the SW concept to derive inertia constant via (5) are compared. In both cases, required data are recorded at the connection buses of SGs.

A. Inertia Estimation via ARMAX Modeling

ARMAX model can be mathematically expressed as

$$\begin{aligned} y[k] + a_1 y[k-1] + ... + a_{n_a} y[k-n_a] = b_1 u[k-1] + \\ ... + b_{n_b} u[k-n_b] + c_1 e[k-1] + ... + c_{n_c} e[k-n_c] \end{aligned} \tag{6}$$

where $y[k]$ is the system response at time instant k; $u[k]$ is the known input of the system, i.e., a disturbance or a probing signal, and $e[k]$ is the unknown input of the system, e.g., noise. Additionally, n_a, n_b and n_c are the order of the autoregressive model, the order of the exogenous input and the order of the moving average model, respectively. The discrete ARMAX model transfer function is given by

$$y[k] = \frac{B(q)}{A(q)}u[k] + \frac{C(q)}{A(q)}e[k] \tag{7}$$

where $B(q)/A(q)$ is the deterministic part, describing the system response to a known input signal. $C(q)/A(q)$ describes the stochastic part, that represents the impact of non-measurable effects on the states of the deterministic part. Polynomials $A(q)$, $B(q)$, and $C(q)$ are defined as

$$\begin{aligned} A(q) &= 1 + a_1 q^{-1} + \cdots + a_{n_a} q^{-n_a} \\ B(q) &= b_1 q^{-1} + \cdots + b_{n_b} q^{-n_b} \\ A(q) &= c_0 + c_1 q^{-1} + \cdots + c_{n_c} q^{-n_c}. \end{aligned} \tag{8}$$

Here, q^{-1} is the backward shift operator. Parameters of (8) can be estimated using a prediction error formulation [2].

ARMAX models can be applied to either ambient or ringdown data. In the former case, the inertial response co-exists with additional dynamic responses, caused by frequency control systems and inter-area oscillations [2], [7], [21]. Therefore, to derive inertia estimates from ambient data, high order ARMAX models are generally required to efficiently approximate the above-mentioned dynamics.

Typical model orders for ambient data analysis range from 2 to 28 [7], [21]. To estimate the parameters of these high order ARMAX models, an analysis window of several seconds is required [7], [21]. Inertia estimates are then determined by computing the step response of the identified ARMAX models and evaluating their initial slope [7], [21]. The length of the analysis window and the order of the ARMAX models depends on the number of power system areas, the adopted control systems, and the noise level.

Inertial response can be specified more accurately using ringdown data. In this case, a second order ARMAX model, i.e., $n_a = n_b = n_c = 2$, can be applied to a short-term analysis interval, containing data captured only a few cycles before and after the disturbance [2]. This way the impact of additional system dynamics, such as frequency control systems and inter-area oscillations, is minimized and accurate inertia estimates are derived [2]. Pre- and post-disturbance windows are presented in Fig. 1. The length of these windows is equal to B_1 and B_2, respectively. Assuming that a disturbance occurs at $t = t_0$, the analysis interval lies on the $[t_0 - B_1,\ t_0 + B_2]$ time range. To properly initialize the ARMAX model, the pre-disturbance window must contain at least a number of samples equal to the order of the ARMAX model. Thus, B_1 can be set to 2. B_2 should be accurately determined [2].

The deterministic part of a second order ARMAX model in the s-domain is

$$G(s) = \frac{\Delta F(s)}{\Delta P(s)} = \frac{\beta_2 s^2 + \beta_1 s + \beta_0}{s^2 + \alpha_1 s + \alpha_0}. \tag{9}$$

$G(s)$ contains the value of the inertia constant but not as an explicit parameter [7]. A simple way to derive the inertia constant is to reduce (9) to a first-order transfer function by identifying and eliminating insignificant states [2], [7]. The reduced order transfer function can be written as

$$G(s) = \frac{\Delta F(s)}{\Delta P(s)} \cong \frac{\beta_r}{s + \alpha_r}. \tag{10}$$

From (3) and (10), the following relationship arise

$$H = -\frac{1}{2\beta_r}. \tag{11}$$

B. Inertia Estimation using the SWM

This method is based on four SWs and is designed to estimate inertia using ringdown data [6]. The required SWs, depicted in Fig. 1, are labeled as P^-, P^+, R^-, R^+. In this notation, P and R denote active power and *RoCoF*, respectively. Superscripts (-) and (+) denote SWs containing pre- and post-disturbance data, respectively.

The SWs act as smoothing filters to eliminate measurement errors [6]. Each window has a length of A data points. Pre- and post-disturbance windows are separated by a width W. Assuming that a disturbance occurs at $t = t_0$, then

$$P^- = \frac{1}{A} \sum_{t=t_0-A}^{t_0} P(t) \tag{12}$$

$$P^+ = \frac{1}{A} \sum_{t=t_0+W}^{t_0+W+A} P(t) \tag{13}$$

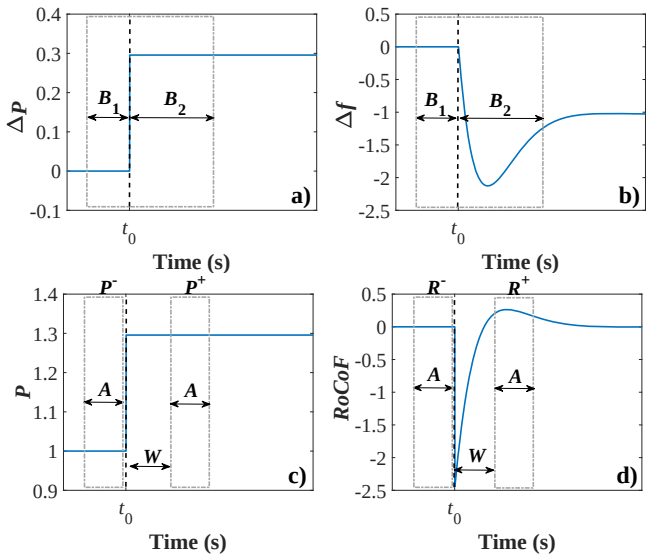

Fig. 1. Data required for the implementation of the examined methods. ARMAX-modelling: a) Active power and b) frequency deviation. SWM: c) Active power and d) $RoCoF$. Settings are not fine-tuned. Figures are only for demonstration purposes.

$$R^- = \frac{1}{A} \sum_{t=t_0-A}^{t_0} \frac{df}{dt}(t) \tag{14}$$

$$R^+ = \frac{1}{A} \sum_{t=t_0+W}^{t_0+W+A} \frac{df}{dt}(t). \tag{15}$$

Using the values of P^-, P^+, R^-, and R^+, the inertia constant is determined by linearizing the swing equation of (5). Specifically, H is computed as

$$H = \frac{1}{2} \frac{P^- - P^+}{R^+ - R^-}. \tag{16}$$

III. Simulations Using a System Frequency Response Model

In this Section, the performance of the examined methods is evaluated via simulations using the system frequency response (SFR) model of [22]. The adopted SFR model constitutes a low-order dynamic equivalent representation of a large power system, dominated by reheat steam turbine generators. The use of the SFR model allows to focus only on power system frequency dynamics [6], [11], [23] in order to quantify the impact of several parameters on the accuracy of the examined methods.

To facilitate the reading, the block structure of the adopted SFR model is depicted in Fig. 2. In this block, p_d is the power of the disturbance in p.u. A negative value for p_d denotes a sudden increase in the total load of the system; a positive value denotes a sudden increase in generation. p_m is the mechanical power in p.u., while p_a stands for the accelerating power. Δ_ω is the p.u. incremental speed. K_m is the mechanical power gain factor, F_H is the fraction of total power generated by the high pressure turbine, and R is the governor droop constant. Finally, T_R is the reheat time constant expressed in s.

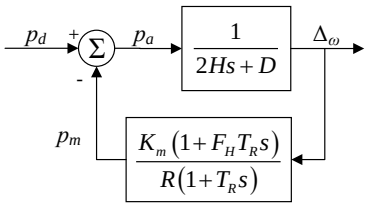

Fig. 2. Adopted SFR model [22].

A. Impact of Window Length

To quantify the impact of the length of the analysis window on the performance of the examined methods, the following procedure is applied: The parameters of the SFR model are set randomly and a ringdown event is analyzed by creating a sudden increase in the total system load. This increase is simulated by setting p_d to a negative value. The resulting dynamic responses are forwarded as inputs to the examined methods to derive inertia constant estimates, i.e., H_{est}. To statistically analyze the performance of the examined methods, a set of 100 MC simulations is performed. In all MC simulations, dynamic responses are generated using a sampling rate equal to 100 samples per second (sps). In each MC simulation the following upper and lower limits for the SFR model parameters are considered: p_d = [-0.5, -0.05], H = [3, 6], D = [0, 2], K_m = [0.9, 0.95], F_H = [0.2, 0.6], T_R = [6, 10], R = [0.05, 0.1].

The impact of the length of the analysis window on the accuracy of the ARMAX method is quantified iteratively following the algorithm of Fig. 3a. Initially, B_2 is set to 6 and the parameters of (9) are estimated. Then, (9) is reduced to (10) by identifying insignificant states and the inertia constant is computed via (11). In the next iteration, B_2 is increased by 1. The procedure terminates when B_2 is 350, i.e., when the length of the post-disturbance window is equal to 3.5 s. In each iteration, actual inertia constant H, i.e., the inertia constant of the SFR model, is compared with the inertia estimate provided by the ARMAX model, using the prediction error PE

$$PE(\%) = \frac{|H - H_{est}|}{H} 100\% \tag{17}$$

here H_{est} denotes the inertia constant estimate.

The impact of W and A on the accuracy of the SWM is quantified using the algorithm of Fig. 3b. Initially, W is set to 2 and A is set to 1. The inertia estimate, H_{est}, is computed using (12) - (16) and compared with the actual inertia constant using (17). In each iteration, W and A are modified. W varies from 2 up to 20, assuming a step equal to 2. A varies from 1 to 40, using a step equal to 1.

The impact of B_2 on the performance of the ARMAX method is quantified in Fig. 4. In this figure the limits of the PE across the 100 MC simulations are presented. 10 instances of the MC simulations are also depicted. As shown, as B_2 increases, PE increases accordingly. This implies that a relatively narrow window is required for the analysis of ringdown data. Indeed, in all MC simulations PE is lower than 5% for windows with length lower than 1.4 s. For higher window lengths, higher PE is observed, indicating performance degradation.

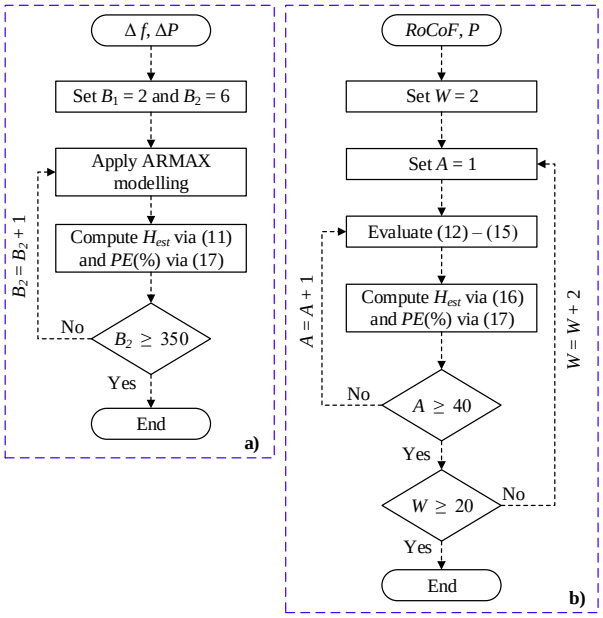

Fig. 3. a) Algorithm used to evaluate the impact of B_2 on the accuracy of ARMAX-modelling. b) Algorithm used to quantify the impact of W and A on the performance of the SWM.

The impact of A and W on the accuracy of the SWM is evaluated in Figs. 5, 6a and 6b. In Fig. 5, results for a specific MC simulation are presented. As shown, PE increases as A and W increase. Similar remarks are also drawn from Figs. 6a and 6b. In these Figs. the limits of the PE across the 100 MC simulations are presented alongside with 10 representative MCs. As shown, the fine tuning of A and W is crucial for the performance of the method, since in case of erroneous settings PE values higher than 5% are observed.

B. Impact of Noise

The previous analysis reveals that fine tuning of B_2, W and A has a significant impact on the accuracy of the examined methods. Therefore, in this subsection the fine tuning of these settings is evaluated under noisy conditions. Specifically, a ringdown event is generated using the SFR model parameters provided in the label of Fig. 5. The dynamic responses are distorted with additive white Gaussian noise (AWGN) assuming signal to noise ratio (SNR) equal to 30 dB, 20 dB,

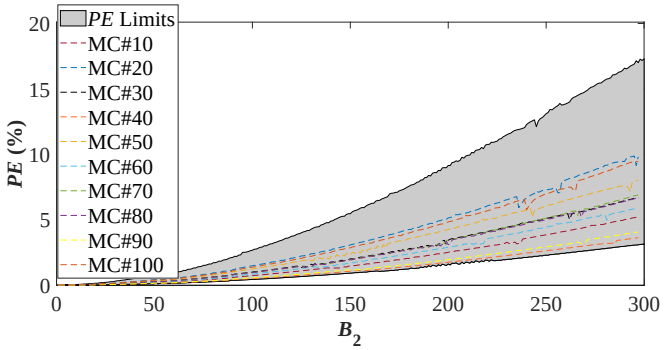

Fig. 4. Impact of B_2 on the accuracy of ARMAX modelling.

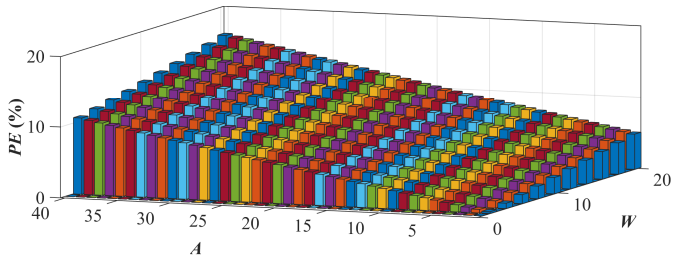

Fig. 5. Impact of A and W on the performance of the SWM. Results for one MC simulation (p_d=-0.2 p.u., H=4 s, D=1, K_m=0.95, F_H=0.3, T_R=8 s, R=0.05).

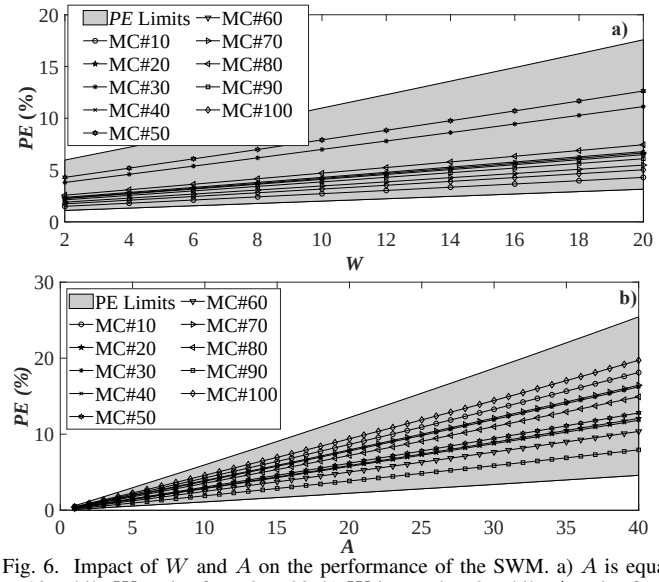

Fig. 6. Impact of W and A on the performance of the SWM. a) A is equal to 10, while W varies from 2 to 20. b) W is equal to 2, while A varies from 1 to 40.

and 10 dB [24]. For each SNR level a set of 100 MC is generated to recreate different instances of noise. For each MC, algorithms of Fig. 3 are executed and optimal values of B_2, W and A are defined. Here, the term "optimal" denotes the values of B_2, W and A that minimize the PE.

The resulting PE is presented in Fig. 7; the optimal values of B_2, W and A are summarized in Fig. 8. As shown in Fig. 7, the ARMAX method provides better estimates compared to the SWM. For instance, for SNR=30 dB, the ARMAX method provides PE lower than 2% in 100% of the examined cases. The SWM provides the same accuracy only in 59% of the examined cases. Similar results are also observed for the cases of the 20 dB and 10 dB. However, it is important to highlight that the ARMAX method may fail to provide inertia estimates in highly noisy conditions. Indeed, for SNR=10 dB, the ARMAX method fails to provide inertia estimates in 7% of the examined cases. In these cases, due to significant noise, unstable transfer functions are obtained. Thus, their parameters cannot be used to derive system inertia.

As shown in Fig. 8a, the optimal value of B_2 generally lies in the range of 6 to 100 samples for SNR=30 dB. However, for lower SNR values, the optimal value of B_2 is highly variable, indicating that predetermined values for this parameter cannot be used. Similar remarks can also be drawn for the SWM. Indeed, for SNR=30 dB, W is always equal to 2, while A

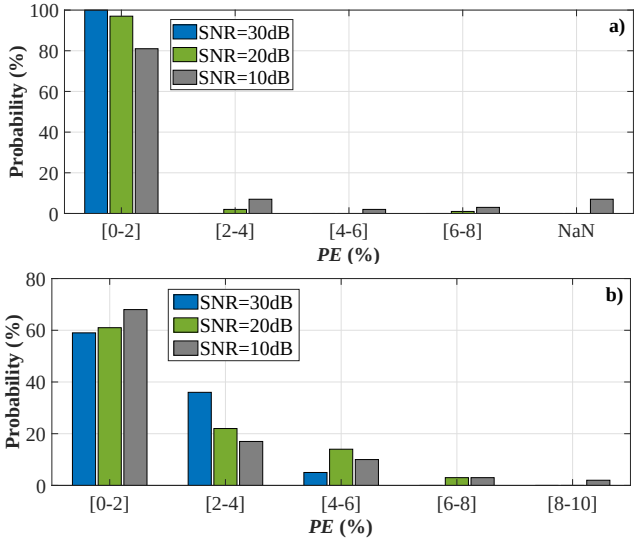

Fig. 7. Impact of noise on PE. a) ARMAX modelling. NaN denotes that the method failed to provide an estimate. b) SWM.

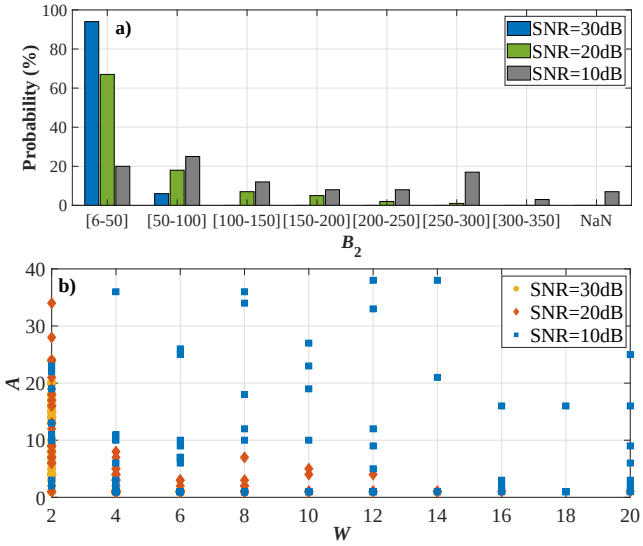

Fig. 8. Impact of noise on the optimal window length. a) ARMAX modelling. b) SWM.

varies from 1 to 20. For lower SNR values both W and A vary significantly. It is clear that predetermined values of W and A cannot be used under noisy conditions, since they will result in significant performance degradation.

C. *Application to Ambient Data*

In Sections III.A and III.B ringdown data were used to evaluate the performance of the examined methods. In this subsection the previous analyzes are repeated using ambient data. For this purpose, 10 minutes of ambient data are generated using the SFR model. In particular, p_d is excited by AWGN, filtered by a low-pass filter with a cut-off frequency of 5 Hz [21]. To replicate small active power fluctuations, caused by the stochastic nature of RESs and power system loads, a SNR equal to 17 dB is assumed for the AWGN used to excite the SFR model [25]. To replicate measurement noise, the resulting dynamic frequency responses are further distorted,

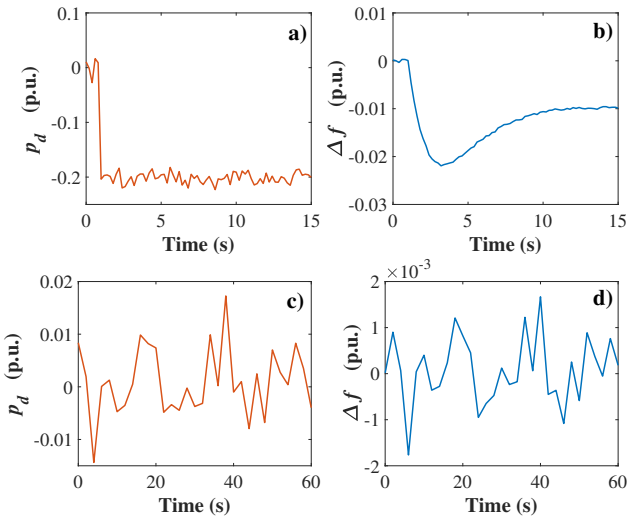

Fig. 9. a) p_d and b) Δf during a representative ringdown event. c) p_d and d) Δf during one minute of ambient data.

TABLE I
PE ON AMBIENT DATA, USING ARMAX MODELING

Observation time	SNR=30dB	SNR=20dB	SNR=10dB
30 s	5.61%	6.95%	11.01%
1 min	2.41%	3.82%	8.01%
2 min	2.03%	3.47%	7.74%
5 min	0.76%	2.23%	6.51%
10 min	0.24%	1.71%	6.06%

on a second stage, assuming three levels of AWGN, namely 30 dB, 20 dB, and 10 dB. To better demonstrate differences between ringdown and ambient data, responses of Fig. 9 are used. More specifically, in Figs. 9a and 9b, p_d and Δf during a ringdown event are plotted, respectively. This event was generated in Section III.B assuming measurement noise with SNR=20 dB. In Figs. 9c and 9d, p_d and Δf under ambient excitation are depicted, respectively. Measurement noise with SNR=20 dB is also considered.

Indicative results for different window lengths and measurement noise levels are summarized in Table I. Note that Table I contains results only for ARMAX modeling, since the SWM cannot be applied to ambient data. In all cases, a second order ARMAX model is used to ensure comparable results. As shown, PE decreases as the window length increases. Therefore, for the analysis of ambient data, a long-term analysis window is required [7], [21]. Based on the conducted simulations, an analysis window of at least 5 minutes is proposed.

IV. Simulations on a Benchmark Power System

The performance of the examined methods is further tested on the IEEE 9-bus test system, shown in Fig. 10. For this purpose, RMS simulations are carried out in Digsilent/Powerfactory using the IEEE 9-bus system model of [26]. Three RESs are also connected to the grid via full scale power converters. RESs are modelled using the Type 4A

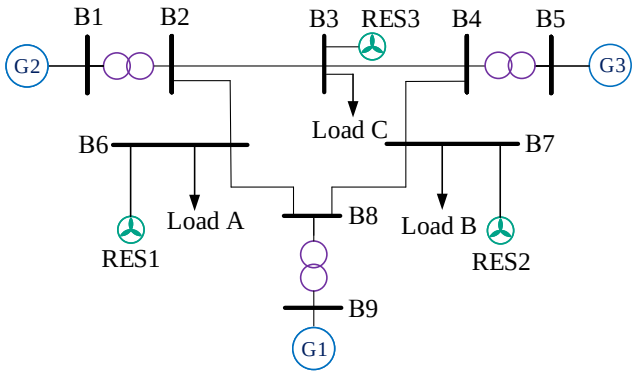

Fig. 10. Single line diagram of the examined system.

model [27]. Four discrete test cases (TCs) are considered in order to evaluate the performance of the examined methods under different penetration levels of RESs. More specifically:

- TC#1: No RESs are considered. The total load demand is covered by the existing SGs.
- TC#2: 10% of the load demand is covered by RES. For this purpose, the power of each RES is set to 10% of the power of the load that is connected to the same bus.
- TC#3: Similar to TC#2. But RES penetration is 20%.
- TC#4: Similar to TC#2. But RES penetration is 30%.

To emulate the decommissioning of SGs, the settings of G2 and G3 are modified in TC#2, TC#3 and TC#4. For this purpose, the power of these SGs is determined in each TC via optimal power flow (OPF) calculations. For each TC a dedicated OPF is conducted, targeting to minimize total system losses. Additionally, the inertia constant of these SGs is reduced proportionally to the corresponding power reduction (reduction compared to TC#1). The equivalent system inertia for the four examined TCs is: $H_{sys}^{TC\#1}$=3.37 s, $H_{sys}^{TC\#2}$=2.57 s, $H_{sys}^{TC\#3}$=2.46 s, and $H_{sys}^{TC\#4}$=2.34 s.

A. Impact of Disturbance Level

For each TC, frequency events are simulated by applying a step-up power increase of Load A. In particular, for each TC, ten ringdown events are considered in total. The disturbance level, i.e., active power imbalance, for each event is presented in Fig. 11. In all cases, frequency and active power responses of all SGs are recorded at a rate of 100 sps.

In all TCs, frequency and active power responses, obtained during the fourth ringdown event (during a 25 MW increase of the total system load), are used as training data and forwarded as inputs to the algorithms of Fig. 3. For each SG, specific values for B_2, W, and A are determined and the individual inertia constants are estimated. With these estimates, the total system inertia, i.e., H_{sys}^{est}, is computed via (4) and the PE between H_{sys} and H_{sys}^{est} is calculated for each TC. PE on training data is summarized in Table II.

The rest of the ringdown events are used as validation data. The validation procedure is performed as follows: frequency and active power responses, obtained during each validation event, are used to determine via (4) the total system inertia. Values of B_2, W, and A are those derived during the training procedure. For each validation event, the PE between H_{sys}

TABLE II
PE ON TRAINING AND VALIDATION DATA SETS

	ARMAX		SWM	
Scenario	**Training**	**Validation**	**Training**	**Validation**
TC#1	0.229 %	0.520 %	0.321 %	0.841 %
TC#2	0.196 %	1.128 %	1.453 %	1.996 %
TC#3	0.171 %	0.751 %	2.097 %	1.987 %
TC#4	0.178 %	0.899 %	1.859 %	2.040 %

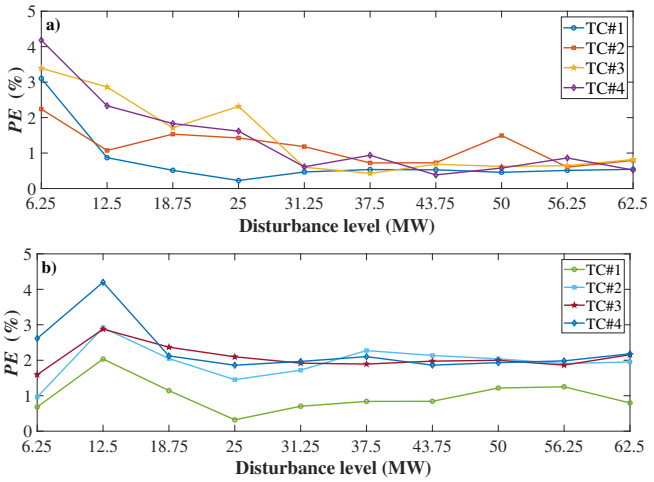

Fig. 11. PE concerning total system inertia along the examined ringdown events. All disturbances are generated by increasing the power of load A.

and H_{sys}^{est} is computed via (17). The mean PE on the validation data set for each TC is summarized in Table II. Additionally, in Fig. 11 the PE across the examined ringdown events is illustrated.

As shown, as the disturbance level increases, the PE of the ARMAX approach tends to decrease. On the other hand, the PE of the SWM is practically not affected from the disturbance magnitude. Additionally, as shown in Table II, both methods provide accurate estimates, while their performance is practically not affected from RES penetration level. Nevertheless, ARMAX method provides lower training and validation errors compared to the SWM.

B. *Impact of Disturbance Location*

To further evaluate the examined methods, new ringdown events are generated for each TC by increasing the active power consumed by Load B. Active power imbalances, used to generate ringdown data, vary from 4.5 MW up to 45 MW, assuming a step of 4.5 MW. Thus, 10 events are simulated for each TC. The resulting dynamic responses are used again to estimate the total system inertia. However, in this case, the training procedure is intentionally omitted and optimal values for B_2, W, and A are not defined. On the contrary, the settings derived in Section IV.A are used. This approach is followed to investigate the impact of the location of the disturbance on the optimal values of B_2, W, and A, and thus on the robustness of the examined methods.

Validation results reveal that in 10% of the examined disturbances, ARMAX modeling results in unstable transfer functions, due to inappropriate window size, thus failing to provide inertia estimates. In the rest of the disturbances, the ARMAX method provides very accurate estimates, since the mean PE across the four TCs is only 1.05%. Optimal values of W and A are not affected significantly by the location of the disturbance. Thus, SWM provides in all cases inertia estimates, exhibiting a mean PE across the four TCs equal to 1.68%.

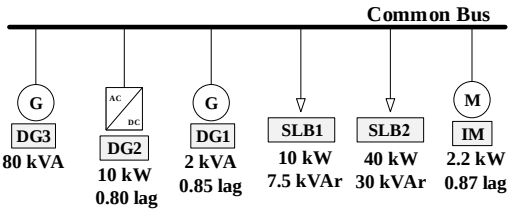

Fig. 12. Experimental setup.

V. APPLICATION TO LABORATORY MEASUREMENTS

In this Section, the performance of the examined methods is evaluated using measurements acquired from a 50 Hz, 400 V laboratory-scale microgrid (MG). The experimental setup is depicted in Fig. 12. The MG operates in islanded mode and consists of three distributed generation (DG) units, two static load banks (SLB) and an induction motor (IM). The nominal characteristics of all MG components are summarized in Fig. 12. In particular, DG1 and DG3 are SGs. DG2 is a converter interfaced unit. All DGs incorporate frequency-active power (f-P) and voltage-reactive power (V-Q) droop control. Nevertheless, DG3 has the main load sharing part, due to its higher power capacity. SLB1 and SLB2 are composed of a 64-step and a 256-step variable resistance and inductance, respectively. Further information concerning the topology and the control systems can be found in [28].

Two TCs are considered, namely TC#A and TC#B. In TC#A DG2 is disconnected; in TC#B DG2 is generating 1 kW at nominal power factor (pf). In both TCs DG1 provides 1 kW/0.75 kVar, SLB1 is 3.5 kW with 0.8 lagging pf, SLB2 is 17 kW with 0.9 lagging pf. The IM is operating at its

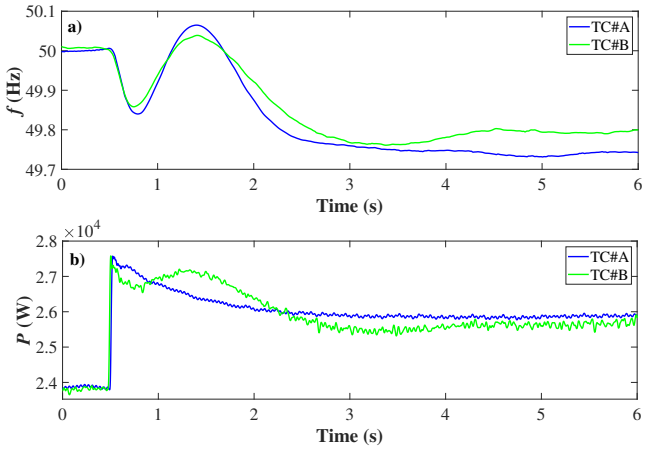

Fig. 13. Laboratory measurements. Recorded a) frequency and b) active power responses.

nominal power. The MG is subjected to a disturbance by applying a 50% load increase to the active and reactive power of SLB1. In both TCs, grid frequency and active power of DG3 are recorded at a data rate of 500 sps. These responses are presented in Fig. 13 and used to estimate the inertia constant of DG3, which is equal to 1 s.

Concerning TC#A, the ARMAX modeling and the SWM result in a PE equal to 6.71% and 3.96%, respectively. Similar results are also observed for TC#B. Indeed, PE for ARMAX modeling is 6.45%, while the PE for the SWM is 3.42%.

VI. Conclusions

In this paper, the performance of two measurement-based inertia estimation techniques is thoroughly evaluated. Towards this objective, the impact of several parameters on the accuracy of the examined methods is investigated and quantified via MC simulations conducted using an SFR model and the IEEE 9-bus test system. Additionally, the applicability of the examined methods is assessed using laboratory measurements.

The conducted analysis reveals that the performance of both methods is considerably affected by the length of the analysis window. Therefore, the fine tuning of B_2, W, and A is required. The optimal length of the analysis window depends on several factors, such as the noise level and the type of data used, i.e. ambient or ringdown. ARMAX modelling provides more accurate inertia estimates under noisy conditions. Additionally, ARMAX models can be applied to both ambient and ringdown data. Concerning the former, a long-term analysis window is required, while for the latter, a short-term interval analysis is more reasonable. The SWM is not appropriate for ambient data analysis. The performance of the ARMAX method is affected by the location of the disturbance, while the SWM is more robust. The performance of both methods is practically not affected by the RES penetration level. Experimental results reveal that both methods can be applied under real-field conditions.

In near future, RESs will provide inertia as ancillary service to the grid. Thus, future work will be conducted to test the performance of the examined methods also for such cases. The impact of switching harmonics, caused from RESs converters, on the accuracy of the examined methods should also be tested. Methodologies to determine in real- or close-to-real-time the optimal length of the analysis window should also be developed to support online inertia estimation.

References

[1] J. C. Smith and C. Clark, "The future's energy mix: The journey to integration [guest editorial]," *IEEE Power Energy Mag.*, vol. 17, no. 6, pp. 19–23, 2019.

[2] L. Lugnani, D. Dotta, C. Lackner, and J. Chow, "Armax-based method for inertial constant estimation of generation units using synchrophasors," *Electr. Power Syst. Res.*, vol. 180, 2020.

[3] E. Orum, M. Kuivaniemi, M. Laasonen, A. I. Bruseth, E. A. Jansson, A. Danell, K. Elkington, and N. Modig, *Future system inertia*. ENTSO-E, Technical Report.

[4] ENTSO-E Technical Group on High Penetration of Power Electronic Interfaced Power Sources, *High penetration of power electronic interfaced power sources and the potential contribution of grid forming converters*. ENTSO-E, Technical Report.

[5] M. Sun, Y. Feng, P. Wall, A. Azizi, J. Yu, and V. Terzija, "On-line power system inertia calculation using wide area measurements," *Int. J. Electr. Power Energy Syst.*, vol. 109, pp. 325–331, 2019.

[6] P. Wall and V. Terzija, "Simultaneous estimation of the time of disturbance and inertia in power systems," *IEEE Trans. Power Del.*, vol. 29, no. 4, pp. 2018–2031, 2014.

[7] K. Tuttelberg, J. Kilter, D. Wilson, and K. Uhlen, "Estimation of power system inertia from ambient wide area measurements," *IEEE Trans. Power Syst.*, vol. 33, no. 6, pp. 7249–7257, 2018.

[8] X. Cao, B. Stephen, I. F. Abdulhadi, C. D. Booth, and G. M. Burt, "Switching markov gaussian models for dynamic power system inertia estimation," *IEEE Trans. Power Syst.*, vol. 31, no. 5, pp. 3394–3403, 2016.

[9] D. P. Chassin, Z. Huang, M. K. Donnelly, C. Hassler, E. Ramirez, and C. Ray, "Estimation of WECC system inertia using observed frequency transients," *IEEE Trans. Power Syst.*, vol. 20, no. 2, pp. 1190–1192, 2005.

[10] F. Allella, E. Chiodo, G. M. Giannuzzi, D. Lauria, and F. Mottola, "On-Line Estimation Assessment of Power Systems Inertia With High Penetration of Renewable Generation," *IEEE Access*, vol. 8, pp. 62 689–62 697, 2020.

[11] D. Zografos, M. Ghandhari, and R. Eriksson, "Real Time Frequency Response Assessment Using Regression," in *2020 IEEE PES Innovative Smart Grid Technologies Europe (ISGT-Europe)*, 2020, pp. 399–403.

[12] J. Zhang and H. Xu, "Online identification of power system equivalent inertia constant," *IEEE Trans. Ind. Electron.*, vol. 64, no. 10, pp. 8098–8107, 2017.

[13] J. Schiffer, P. Aristidou, and R. Ortega, "Online estimation of power system inertia using dynamic regressor extension and mixing," *IEEE Trans. Power Syst.*, vol. 34, no. 6, pp. 4993–5001, 2019.

[14] P. M. Ashton, C. S. Saunders, G. A. Taylor, A. M. Carter, and M. E. Bradley, "Inertia estimation of the gb power system using synchrophasor measurements," *IEEE Trans. Power Syst.*, vol. 30, no. 2, pp. 701–709, 2015.

[15] D. Zografos and M. Ghandhari, "Power system inertia estimation by approaching load power change after a disturbance," in *2017 IEEE Power Energy Society General Meeting*, 2017, pp. 1–5.

[16] D. Zografos, M. Ghandhari, and R. Eriksson, "Power system inertia estimation: Utilization of frequency and voltage responses after a disturbance," *Electr. Power Syst. Res.*, vol. 161, pp. 52–60, 2018.

[17] T. Inoue, H. Taniguchi, Y. Ikeguchi, and K. Yoshida, "Estimation of power system inertia constant and capacity of spinning-reserve support generators using measured frequency transients," *IEEE Trans. Power Syst.*, vol. 12, no. 1, pp. 136–143, 1997.

[18] D. del Giudice and S. Grillo, "Analysis of the Sensitivity of Extended Kalman Filter-Based Inertia Estimation Method to the Assumed Time of Disturbance," *Energies*, vol. 12, no. 3, 2019.

[19] P. Wall, F. Gonzalez-Longatt, and V. Terzija, "Estimation of generator inertia available during a disturbance," in *2012 IEEE Power and Energy Society General Meeting*, 2012.

[20] P. M. Anderson and A. A. Fouad, *Power system control and stability*. 2nd ed. Piscataway, NJ, USA: IEEE, 2003.

[21] F. Zeng, J. Zhang, G. Chen, Z. Wu, S. Huang, and Y. Liang, "Online Estimation of Power System Inertia Constant Under Normal Operating Conditions," *IEEE Access*, vol. 8, pp. 101 426–101 436, 2020.

[22] P. M. Anderson and M. Mirheydar, "A low-order system frequency response model," *IEEE Trans. Power Syst.*, vol. 5, no. 3, pp. 720–729, 1990.

[23] A. Fernández-Guillamon, A. Vigueras-Rodriguez, and A. Molina-Garcia, "Analysis of power system inertia estimation in high wind power plant integration scenarios," *IET Renew. Power Gener.*, vol. 13, no. 15, pp. 2807–2816, 2019.

[24] IEEE Task Force on Identification of Electromechanical Modes, *Identification of electromechanical modes in power systems*. IEEE Power & Energy Society, 2012, PES-TR15.

[25] V. S. Peric and L. Vanfretti, "Power-System Ambient-Mode Estimation Considering Spectral Load Properties," *IEEE Trans. Power Syst.*, vol. 29, no. 3, pp. 1133–1143, 2014.

[26] https://www2.kios.ucy.ac.cy/testsystems/.

[27] IEC Wind Energy Generation Systems – Part 27-1: Electrical Simulations Models – Generic Models, 2020.

[28] T. A. Papadopoulos, P. N. Papadopoulos, G. K. Papagiannis, P. Crolla, A. J. Roscoe, and G. M. Burt, "Dynamic performance of a low voltage microgrid with droop controlled distributed generation," in *2013 IEEE Power Energy Society General Meeting*, 2013, pp. 1–5.